Tetrahedron 71 (2015) 7583–7592

Contents lists available at ScienceDirect

Tetrahedron

journal homepage: www.elsevier.com/locate/tet

# Synthesis, structural and conformational analysis, and IR spectra of ethyl 4-chloro-7-iodoquinoline-3-carboxylate

P.C. Horta [a], M.S.C. Henriques [b], N. Kuş [c,d], J.A. Paixão [b], P.M. O'Neill [e], M.L.S. Cristiano [a,*], R. Fausto [c,*]

[a] CCMAR and Department of Chemistry and Pharmacy, University of Algarve, Faro, Portugal
[b] CFisUC, Department of Physics, University of Coimbra, Portugal
[c] Department of Chemistry, University of Coimbra, Portugal
[d] Department of Physics, Anadolu University, Eskişehir, Turkey
[e] Department of Chemistry, University of Liverpool, United Kingdom

ARTICLE INFO

*Article history:*
Received 3 July 2015
Received in revised form 30 July 2015
Accepted 31 July 2015
Available online 6 August 2015

*Keywords:*
4-Chloro-7-iodoquinoline-3-carboxylate
IR matrix isolation spectroscopy
Temperature dependent neat solid state IR spectroscopy
Single crystal X-ray diffraction
B3LYP/LANL2DZ+cc-pVDZ
Conformational analysis

ABSTRACT

In this work, we report the synthesis of a novel quinoline derivative, ethyl 4-chloro-7-iodoquinoline-3-carboxylate (CIQC), and its structural, conformational and vibrational characterization. The compound was studied in its neat solid phases (crystalline and low-temperature amorphous phases) and as an isolated species in a cryogenic argon matrix (at ~15 K). Infrared spectroscopy and single crystal X-ray diffraction were the chosen experimental techniques. The conformational space and the vibrational spectra of the isolated molecules of the compound were also investigated theoretically at the B3LYP/LANL2DZ+cc-pVDZ level of approximation.

The CIQC molecule exists in four different conformers, with predicted populations of 42:25:17:16% at room temperature (rt). The rt equilibrium conformational mixture was successfully trapped in an argon matrix, at 15 K, and the vibrational signatures of the conformers were determined. Upon annealing of the matrix of the compound at higher temperatures (~40 K), conversion of the higher energy forms into the most stable conformer was found to take place, in consonance with the low predicted barriers for conformational isomerization. Sublimation of the host matrix argon atoms (at ~43 K) led to production of a low-temperature amorphous state of CIQC, containing the lowest but also the higher energy conformers. At $T$ ~233–243 K, the amorphous rearranged to the crystalline state, whose molecular unit corresponds to the most stable CIQC conformer, as shown both by infrared spectroscopy and single crystal X-ray diffraction.

At room temperature CIQC crystallizes in the hexagonal $P6_3/m$ space group, with $a=b=17.7928(2)$ Å, and $c=6.9830(1)$ Å. The molecules lie on a crystallographic mirror plane and are stacked in layers along the $c$-axis. The main packing motif consists of a group of three molecules, related by a three-fold rotation, joined together by weak C–H ··· O hydrogen bonds.



## 1. Introduction

Quinolines have attracted intense research for several decades and the interest in this class of compounds does not appear to fade. One important reason for this perennial interest lies in the applications of the quinoline chemotype in medicine. Many quinoline derivatives are known for their pharmacological properties targeting a variety of diseases, e.g., cancer,[1] hepatitis,[2,3] anti-HIV,[4] herpes,[5] immunodepression,[6] tuberculosis[7] or malaria.[8–11]

Malaria remains one of the most deadly parasitic infectious diseases in the world.[12] The growing emergence of resistance against conventional antimalarials, including ACT's, urges the search for novel and better antiplasmodial drugs, preferably directed to new targets.[13–15]

The approval of Malarone® for the treatment and prevention of multidrug resistant malaria validated the *bc1* protein complex of *Plasmodium falciparum* as target for developing new antimalarial drugs. The *bc1* complex is a homodimeric transmembrane protein responsible for the transfer of electrons from ubiquinol to cytochrome *c*, concomitantly with the vectorial translocation of protons across the inner mitochondrial membrane[16,17] and has been considered as an important target for antiplasmodial drug design. It

* Corresponding authors. E-mail addresses: mcristi@ualg.pt (M.L.S. Cristiano), rfausto@ci.uc.pt (R. Fausto).

http://dx.doi.org/10.1016/j.tet.2015.07.076
0040-4020/

has been proposed that quinolone 3-esters **1** (Scheme 1) target the $Q_o$ site of the enzyme in the *bc1* complex, leading to a drop of mitochondrial function (relevant to provide intermediates for pyrimidine and ATP synthesis),[18,19] collapse of the *trans*-membrane electrochemical potential and parasite death.[20] However, compounds **1** present some liabilities, such as poor solubility (poor pharmacokinetic profile).

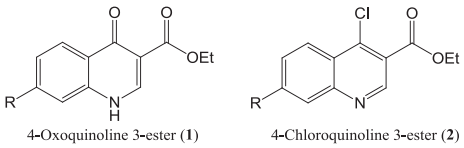


**Scheme 1.** General structure for target 7-substituted quinolones 3-esters (**1**) and for 7-substituted 4-chloroquinolines 3-esters (**2**).

It is proposed that structure-based optimization of **1** may be achieved by altering the nature of the substituent in position 7. As such, a representative library of compounds **1** for SAR studies is required, and these studies should provide compounds with improved pharmacological profile that have the potential to be taken forward as drug leads. Ethyl 4-chloro-7-iodoquinoline-3-carboxylate (**2**, CIQC—Scheme 2), proved to be instrumental as intermediate for easy access to a range of new quinolone 3-esters **1**.

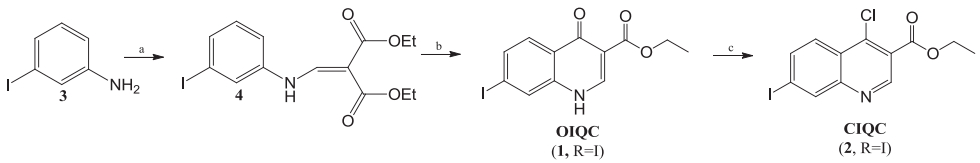


**Scheme 2.** Synthetic approach to ethyl 4-oxo-7-iodoquinoline-3-carboxylate, OIQC (**1**, R=I) and to ethyl 4-chloro-7-iodoquinoline-3-carboxylate, ClQC (**2**, R=I). Conditions: (a) 110 °C, o.n.; (b) Dowtherm A, 250 °C, 3 h; (c) $POCl_3$, 97 °C, o.n.

We report the synthesis and detailed structure of CIQC. The monomeric structure of CIQC was studied using the matrix isolation technique coupled to infrared spectroscopy and contemporary molecular orbital calculations. The structure of crystalline CIQC was studied by X-ray crystallography and vibrational spectroscopy.

## 2. Experimental and computational methods

### 2.1. Synthesis

*2.1.1. General methods.* All reagents and solvents were purchased from commercial sources and used as received. When necessary, solvents were freshly distilled from appropriate drying agents before use. The reactions were monitored by TLC, using silica gel F254 plates. Whenever required, inorganic solids were removed by filtration through a layer of Celite® 512 medium. NMR spectra for compounds, in appropriate solvents ($D_6$-DMSO or $D_1$-chloroform), were measured using TMS as internal reference ($\delta$=0.0 ppm). Chemical shifts ($\delta$) are described in parts per million (ppm). Splitting patterns are designated as s (singlet), d (doublet), t (triplet), q (quartet) and m (multiplet). NMR spectra for target compounds, operated at 400 and 100 MHz, for $^1H$ and $^{13}C$, respectively, are provided as Supplementary Data (Figs. S1–S5). Melting points were recorded on a Stuart Scientific SMP3 melting point apparatus and are uncorrected. Mass spectra were recorded using Micromass LCT, via electrospray (ES), and are provided as Supplementary Data (Figs. S6–S8). Elemental analyses (CHNS) were performed at the University of Liverpool, Department of Chemistry.

*2.1.2. Preparation of diethyl 2-((3-iodo-phenylamino)methylene) malonate (**4**).* 3-Iodo-aniline **3** (5 mL; 41.6 mmol) and diethyl ethoxymethylenemalonate (9.4 mL; 45.7 mmol) were stirred at 110 °C, overnight. The reaction mixture was cooled, hexane was added, and the precipitate was collected by filtration to give diethyl 2-((3-iodo-phenylamino)methylene)malonate **4** as white solid (97%). Melting range 86.4–87.9 °C. $^1H$ NMR (400 MHz, $CDCl_3$) $\delta$ 10.97 (d, $J$=13.5 Hz, 1H), 8.47–8.42 (m, 1H), 7.51–7.46 (m, 2H), 7.11–7.08 (m, 2H), 4.28 (dq, $J$=19.1, 7.1 Hz, 4H), 1.36 (dt, $J$=16.8, 7.1 Hz, 6H). $^{13}C$ NMR (100 MHz, $CDCl_3$) $\delta$ 168.9, 151.3, 140.4, 133.8, 131.2, 126.0, 116.4, 95.0, 94.6, 60.6, 60.3, 14.4, 14.2. MS ($ES^+$) $m/z$ 412 $(M+Na)^+$ Acc. mass found: 412.0020, calculated 412.0022 for $C_{14}H_{16}INO_4$ Na.

*2.1.3. Preparation of ethyl 4-oxo-7-iodo-quinoline-3-carboxylate (OIQC, **1**).* Diethyl 2-((3-iodo-phenylamino)methylene)malonate **4** (10.14 g; 26.1 mmol) was suspended in Dowtherm A (80 mL), under a nitrogen atmosphere, and the mixture was heated at 250 °C for 3 h. The reaction mixture was cooled to room temperature. The solid precipitate was filtered, washed with hexane and diethyl ether, and dried to afford ethyl 4-oxo-7-iodo-quinoline-3-carboxylate OIQC, 1 (R=I) as white solid (44%). Melting range 306–308 °C. $^1H$ NMR (400 MHz, $(CD_3)_2SO$) $\delta$ 8.56 (s, 1H), 8.15 (s, 1H), 8.02 (s, 1H), 7.88 (d, $J$=8.5 Hz, 1H), 7.73 (d, $J$=8.4 Hz, 1H), 4.25–4.16 (q, $J$=7.1 Hz, 2H), 1.27 (t, $J$=7.1 Hz, 3H). MS ($ES^+$) $m/z$ 366 $(M+Na)^+$ Acc. mass found: 365.9591; calculated for $C_{12}H_{10}INO_3Na$: 365.9603. CHNS for $C_{12}H_{10}INO_3$ requires C 42.01%, H 2.94%, N 4.08%, found C 42.17%, H 2.84%, N 3.95%.

*2.1.4. Preparation of ethyl 4-chloro-7-iodo-quinoline-3-carboxylate (CIQC, **2**).* Ethyl 4-oxo-7-iodo-quinoline-3-carboxylate OIQC (0.7 g; 2.04 mmol) was suspended in phosphoryl chloride (5 mL), under a nitrogen atmosphere, and the resulting mixture was refluxed at 97 °C overnight. The mixture was cooled to room temperature, poured into a beaker of ice, stirred for 1 h and then extracted with chloroform. Organic layers were collected, dried under $MgSO_4$ and the solvent was removed to afford ethyl 4-chloro-7-iodo-quinoline-3-carboxylate CIQC, **2** (R=I) as yellow solid (95%). Melting range 269–271 °C. $^1H$ NMR (400 MHz, $CDCl_3$) $\delta$ 9.19 (s, 1H), 8.60 (s, 1H), 8.12 (d, $J$=8.9 Hz, 1H), 7.99 (d, $J$=1.6 Hz, 1H), 4.50 (q, $J$=7.1 Hz, 2H), 1.47 (t, $J$=7.1 Hz, 3H. $^{13}C$ NMR (100 MHz, $CDCl_3$) $\delta$ 164.18, 150.95, 149.75, 138.69, 137.29, 126.59, 125.52, 123.33, 99.18, 62.28, 14.25. MS ($ES^+$) $m/z$ 361.9/363.9 $[M+H]^+$. CHNS for $C_{12}H_9ClINO_2$ requires C 39.86%, H 2.51%, N 3.87%; found C 39.28%, H 2.73%, N 3.56%.

### 2.2. X-ray diffraction studies

A single crystal X-ray Diffraction (XRD) study of the title compound (CIQC) was performed at room temperature on a Bruker APEXII diffractometer using graphite monochromatized Mo $K_\alpha$ radiation ($\lambda$=0.71073 Å). The unit cell derived from the first 36 CCD frames was found to be hexagonal with cell parameters, $a=b$=17.7928(2) Å, $c$=6.98300(10) Å, $\alpha=\beta$=90°, $\gamma$=120°. Systematic absences pointed to the structure belonging to either $P6_3$ or $P6_3/m$ space groups, the latter being confirmed during structure solution and refinement. The refined structural model gave a final $R_1$ factor

of 0.0264 (for 1188 reflections with $I>2\sigma$) and $R_{all}$ of 0.0496 for all 1733 reflections and 111 parameters (full anisotropic model with H atoms riding on their parent atoms). Bond lengths and angles are within the expected range of values. Further details on data collection, structure refinement and full tables of interatomic distances, valence and torsion angles are given in the Supplementary Data (Crystallographic Data Section, Tables CDS1–CDS9). The crystal structure has been deposited at the Cambridge Crystallographic Data Centre (deposition number CCDC 1406711).

### 2.3. Matrix preparation and infrared spectroscopy

Isolation of the compound in solid argon was achieved by sublimating the solid compound in a specialized thermoelectrically-heatable mini-oven assembled inside the cryostat, and co-depositing the vapors of the compound with argon (N60, supplied by Air Liquide), coming out from a separate line, onto a CsI window kept at 15 K. The obtained matrices were enough diluted (matrix:sample ratio >1000), so that they contain only monomers of the compound. Annealing of the matrices was undertaken in steps of 1°, until evaporation of the argon host (at ~43 K), and in steps of 5°, after that temperature. Evaporation of the host matrix atoms allowed obtaining an amorphous solid of the compound, which could later be crystallized at a temperature of ~233–243 K. The crystal was then *re*-cooled down to 17 K and its infrared spectrum collected.

The used low temperature set up includes, as main component, an APD Cryogenics closed-cycle helium refrigeration system, with a DE-202A expander. The temperature was measured directly at the sample holder, using a silicon diode sensor connected to a digital temperature controller (Scientific Instruments, Model 9650-1), which provides accuracy of 0.1°.

The IR spectra were recorded in the 4000–450 $cm^{-1}$ range with 0.5 $cm^{-1}$ resolution, on a Thermo Nicolet 6700 FTIR spectrometer, equipped with a deuterated triglycine sulfate (DTGS) detector and a KBr beamsplitter.

### 2.4. Computational methods

The quantum chemical calculations were performed using Gaussian 09.[21] Geometries were fully optimized at the DFT level of approximation, using the B3LYP functional,[22–24] together with the cc-pVDZ basis set, for C, H and Cl atoms, and the LANL2DZ (Los Alamos National Laboratory 2 Double-ζ) effective core potential (ECP) on iodine.[25–27] The harmonic vibrational wavenumbers were obtained at the same level of theory and scaled by 0.978, to correct them for the shortcomings of the applied methodology (mainly for anharmonicity).

## 3. Results and discussion

### 3.1. Synthesis

Quinolone 3-esters **1** may be prepared from an α,β-unsaturated ester derivative of aniline (usually a malonate derivative, **4**; Scheme 2) through a thermally driven intramolecular cyclization known as the Gould-Jacobs methodology.[28] In the thermally driven cyclization it is proposed that the phenyl ring acts as nucleophile, attacking the carbon of the ester carbonyl group.[28] However, this approach presents limitations, mostly related to the high temperature (above 225 °C) required for reaction. The reaction is concentration dependent and thermal degradation may occur.[5] Additionally, most quinolones exhibit low solubility, leading to difficulties in extraction and purification. As such, an alternative methodology, based in the synthesis of 4-chloroquinoline **2** intermediates, was proposed. 4-Chloroquinolines **2** are more easily solubilized and isolated and may be, subsequently, converted into the corresponding quinolones. ClQC represents a versatile building block from which several compounds can be synthesized, introducing chemical diversity at positions 4 and 7: the 4-chloro-7-iodoquinoline core may be easily transformed into a range of 4-quinoline derivatives through nucleophilic displacement of the chloride anion, and may also serve as substrate for the preparation of a library of 7-substituted derivatives, for example, by Suzuki coupling.

The synthetic strategy to ClQC is devised in Scheme 2. Firstly, 3-iodoaniline **3** was converted into the diethylmalonate derivative **4** (see characterization in Figs. S1, S2 and S6, Supplementary Data). Thermal cyclization of **4** (using Dowtherm A) produced quinolone OIQC. To improve the physicochemical profile, OIQC was submitted to chlorination with $POCl_3$, affording ClQC as isolated product. OIQC and ClQC were isolated and characterized (see Section 2.1 and Supplementary Data).

### 3.2. Potential energy surface characterization

The 4-chloro-7-iodoquinoline-3-carboxylate (ClQC) molecule has three degrees of internal rotation that may result in different conformers. These correspond to rotations about the two C–O bonds (carboxylic and ester) and around the C–C bond connecting the carboxylic ester substituent to the ring system (see Fig. 1). Structures with the carboxylic ester moiety adopting the *trans* configuration (O=C–O–C dihedral in the 180° region) can be expected to be high-energy forms, due to steric hindrance resulting from the close proximity between the ethyl-ester fragment and the ring substituents at the *ortho* position to the carboxylic ester group (H, Cl). In addition, it is well-known that the *trans* configuration of a carboxylic ester fragment is in general energetically unfavored in relation to the *cis* one (O=C–O–C dihedral in the 0° region).[29,30] Taking this into account, the *cis* conformation around the carboxylic C–O bond was assumed in the performed analysis of the potential energy surface of ClQC. Under this restriction, the conformationally flexible internal torsional coordinates of the molecule reduce to only two. Scanning of these two coordinates (see Figs. S9 and S10, in the Supplementary Data) resulted in four different minimum energy structures, which are depicted in Fig. 1. The calculated relative energies (with and without zero-point correction) and Gibbs energies (at 298.15 K) of these four conformers are provided in Table 1.

According to the calculations, the two conformers where the carbonyl oxygen atom is turned to the same side of the chlorine atom (*sa* and *sg*) are slightly more stable than those where the chlorine atom faces the ester oxygen atom (*aa* and *ag*). This is in consonance with a more important steric relevance of the ester oxygen atom compared to the carbonyl oxygen atom, as shown before for other molecules.[31,32] In turn, for each pair of conformers showing the same arrangement of the carboxylic ester substituent in relation to the ring system (i.e., the *sa*/*sg* and *aa*/*ag* pairs), the form exhibiting the ester group in the *anti* conformation corresponds to the more stable form. This result follows also the general trend for ethyl carboxylic esters.[33–35]

The most stable conformer of ClQC is then the *sa* form. Nevertheless, the calculated electronic energies for the four conformers are rather similar, with the less stable form (*ag*) being only 0.92 kJ $mol^{-1}$ higher in energy than the most stable one (see Table 1). Consideration of the zero-point energies and thermal corrections slightly stabilizes the two conformers exhibiting the *anti* ester group (*aa* and, specially, the most stable *sa* form) relatively to the *gauche* forms. At 298.15 K, the calculated Gibbs relative energies lead to expected populations for *sa*, *aa*, *sg* and *ag* of 41.8, 15.7, 25.2 and 17.3%, respectively, i.e., all four conformers can be expected to

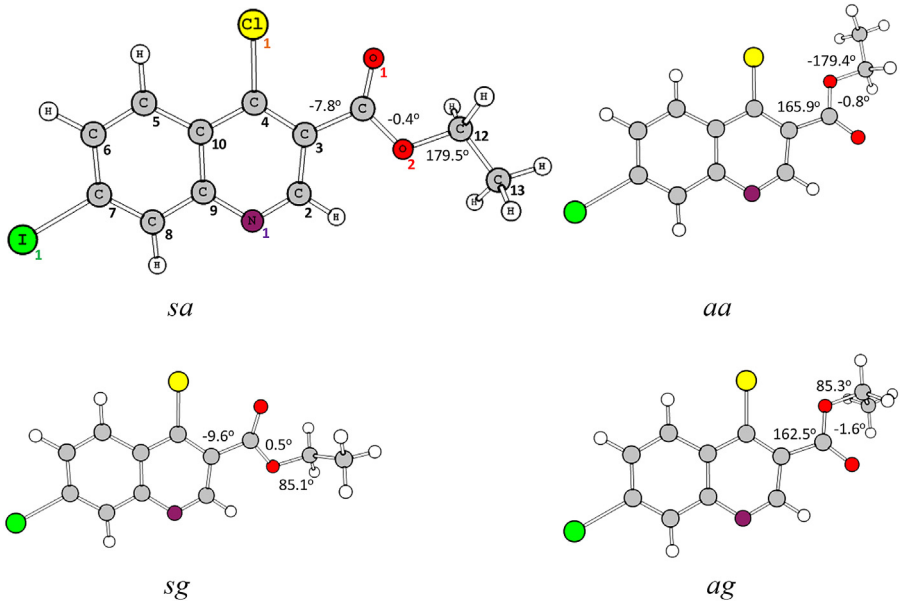


**Fig. 1.** Optimized geometries for conformers of ClQC, with adopted atom numbering. The optimized values of the C–C–C=O, O=C–O–C and C–O–C–C dihedrals (°) are indicated.

**Table 1**
B3LYP/LANL2DZ+cc-pVDZ calculated relative electronic energies ($\Delta E$/kJ mol$^{-1}$), zero-point corrected energies ($\Delta E_0$/kJ mol$^{-1}$) and Gibbs energies ($\Delta G°$/kJ mol$^{-1}$) for minima of ClQC, and expected room temperature (298.15 K) gas phase populations ($p^{298.15}$/%)

| Conformer[a] | ΔE | $\Delta E_0$ | ΔG° | $p^{298.15}$[b] |
|---|---|---|---|---|
| *sa* | 0.00 | 0.00 | 0.00 | 41.8 |
| *aa* | 0.61 | 0.77 | 2.43 | 15.7 |
| *sg* | 0.43 | 1.23 | 2.97 | 25.2 |
| *ag* | 0.92 | 1.64 | 3.90 | 17.3 |

[a] See Fig. 1 for structures of the conformers.
[b] Conformers *sa* and *aa* considered to be represented by a single structure (see text); conformers *sg* and *ag* have two equivalent-by-symmetry forms (*sg*±; *ag*±), and their degenerescence was set equal to 2.

have significant populations in the room temperature gas phase equilibrium.

A note shall be made here regarding the structures of the two conformers exhibiting the *anti* ester group (*sa* and *aa*). As shown in Fig. 1, the calculations yield minimum energy geometries for these two conformers where the heavy atoms backbone is slightly non-planar (the larger deviation from planarity occurs for the very flexible C–C–C=O coordinate, which has very low predicted torsional frequencies: 11 and 15 cm$^{-1}$, for *sa* and *aa*, respectively). Thus, two equivalent-by-symmetry minima exist for each form. However, for both *sa* and *aa* conformers, the energy difference between the found minima and the nearby structure exhibiting a planar skeleton is extremely small (below 0.01 kJ mol$^{-1}$), being below the zero-point level associated with the C–C–C=O torsional coordinate. Under these circumstances, the experimentally relevant geometries for the *sa* and *aa* conformers correspond to the most probable structure linked to each potential energy well, i.e., to the structure with planar skeleton symmetrically positioned in relation to the minima. In practical terms, this grants for both *sa* and *aa* conformers a $C_s$ symmetry.

The barriers for interconversion between the conformers of ClQC have also been calculated. As shown in Fig. S9, rotations about the C–O ester bond for the two possible configurations of the carboxylic ester substituent in relation to the ring system (*syn* and *anti*) yield practically identical energy profiles. The $sg^{\pm} \rightarrow sa$ and $ag^{\pm} \rightarrow aa$ energy barriers were calculated to be small (2.2 and 2.7 kJ mol$^{-1}$, respectively), whereas the barriers interconnecting the equivalent-by-symmetry *gauche* forms, $sg^{+} \leftrightarrow sg^{-}$ and $ag^{+} \leftrightarrow ag^{-}$ are considerably larger (28.7 and 27.8 kJ mol$^{-1}$, respectively), since these latter are associated with sterically hindered transition states (see Fig. 1 and Fig. S9). Internal rotation about the C–C bond connecting the carboxylic ester substituent to the ring system interconverts the pairs of conformers *aa*/*sa* and $ag^{\pm}/sg^{\pm}$ (see Fig. S10). The calculations yield energy barriers for the $aa \rightarrow sa$ and $ag^{\pm} \rightarrow sg^{\pm}$ processes equal to 12.1 and 12.4/12.2 kJ mol$^{-1}$, respectively.

With exception of the direct conversion between the equivalent-by-symmetry *gauche* forms, conformational isomerizations between the various conformers of ClQC have enough low energy barriers to be expected to be possible to induce by warming of a cryogenic argon matrix of the compound to an experimentally accessible temperature (argon evaporates at a temperature slightly above 40 K).[36] As shown in detail in the next section, these predictions were fully confirmed experimentally.

An additional point should be commented here. Since the gas phase predicted $sg^{\pm} \rightarrow sa$ and $ag^{\pm} \rightarrow aa$ energy barriers are in fact quite low (2.2 and 2.7 kJ mol$^{-1}$, respectively) the possibility of conversion of the *gauche* conformers into their corresponding *anti* forms during matrix deposition has to be considered. However, studies on other ethyl carboxylic esters exhibiting similar energy barriers for the *gauche* → *anti* ethyl ester isomerization have demonstrated that both types of conformers can indeed be trapped in cryogenic matrices rather efficiently.[33]

### 3.3. Matrix isolation infrared spectroscopy studies

The infrared spectrum of ClQC isolated in an argon matrix (15 K) is presented in Fig. 2. In this figure, simulated infrared spectra built using the B3LYP/LANL2DZ+cc-pVDZ calculated data for the ClQC conformers are also shown. Two simulated spectra are depicted, one corresponding to the individual spectrum of the most stable *sa* conformer, and the other being the sum of the spectra of the four conformers weighted by their estimated room temperature equilibrium populations (see Table 1). The calculated spectra for the different conformers are provided in Fig. 3 and Table S1 (Supplementary Data).

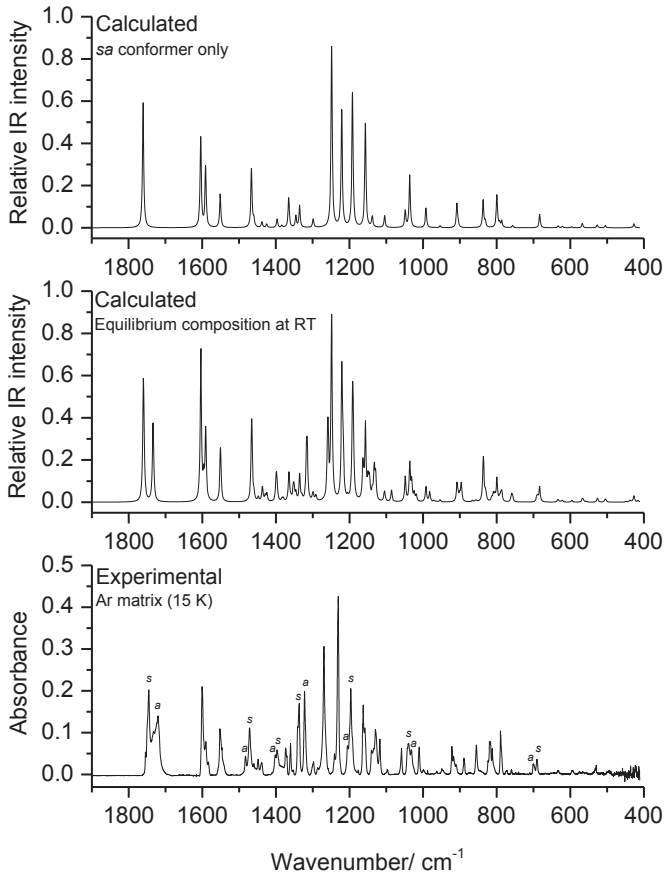


**Fig. 2.** *From bottom to top*: observed infrared spectrum of ClQC isolated in solid argon (15 K) from the vapour at room temperature (rt), and simulated infrared spectra using the B3LYP/LANL2DZ+cc-pVDZ calculated data for the expected equilibrium conformational mixture at rt (*sa*:*aa*:*sg*:*ag*=41.8:15.7:25.2:17.3%), and for the most stable conformer (*sa*) only. In the experimental spectrum, the most intense characteristic bands of *s*- and *a*-type conformers are indicated by the letters '*s*' and '*a*' (see Table 2 for detailed assignments).

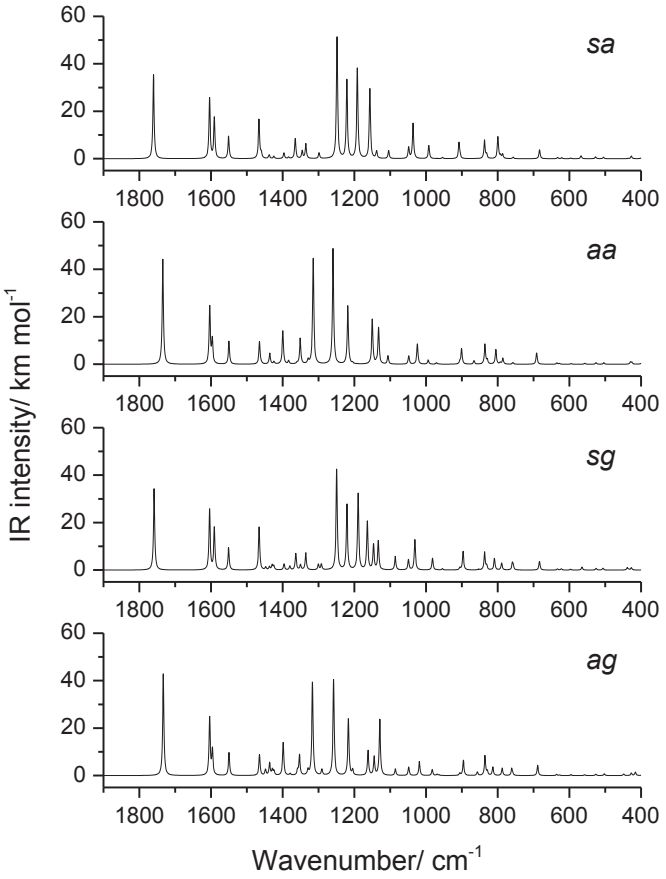


**Fig. 3.** B3LYP/LANL2DZ+cc-pVDZ calculated infrared spectra for *sa*, *aa*, *sg* and *ag* conformers of ClQC, **2** (R=I). The bands were simulated by Lorentzian functions centered at the calculated frequencies (scaled by 0.978) and with a full-width at half-maximum (fwhm) of 2 $cm^{-1}$; the area under each band corresponds to its calculated IR intensity.

It is clear from Fig. 2 that the simulated spectrum constructed assuming the trapping of the equilibrium conformational mixture existing in the gas phase prior to deposition agrees rather well with the experimental spectrum, while that of the most stable *sa* conformer alone does not fit properly the experimental pattern. This is evident all along the different spectral regions, but it is particularly noticeable in the C=O stretching region, between 1700 and 1800 $cm^{-1}$, where the experimental spectrum shows essentially a double-band structure as in the simulated spectrum of the conformational mixture (in opposition to the single band in the sole spectrum of *sa*), and between 1000 and 1400 $cm^{-1}$, where both the number and relative intensities of the observed bands is much better fitted by the theoretical spectrum of the conformational mixture than by the individual spectrum of conformer *sa*.

Besides demonstrating that the conformational composition of ClQC present in the gas phase prior to deposition could be trapped in the cryogenic matrix without substantial conformational conversion during matrix deposition (i.e., that no significant conformational cooling[37–39] has occurred), these results allow also to conclude that the used theoretical model yields a good estimation of the relative energies of the conformers, and also of their vibrational spectra. Such conclusions are reinforced by the results of the performed temperature variation studies, as described below.

Fig. 4 shows the difference spectrum obtained by subtracting the spectrum of the as-deposited ClQC argon matrix (15 K) from the spectrum obtained after warming the matrix until 40 K (in steps of 1 K). The observed changes are consistent with occurrence of conformational isomerization (in fact, the changes started to be noticeable already at $T$=25 K). However, the detailed analysis of the conformational transformations taking place upon warming of the matrix is not straightforward, because the vibrational signatures of the conformers exhibiting the same orientation of the ethyl carboxylic ester substituent in relation to the ring system (i.e., the pairs *sa*/*sg* and *aa*/*ag*) are very similar. This is clearly shown in Fig. 3. In fact, from the practical point of view, the major complication results from the similarity of the spectra of the most stable *sa* conformer and of the *sg* form. The extensive coincidence of bands of these two forms makes difficult to scrutinize the spectral effects of the expected *sg*→*ag* conversion, since these are mostly dependent on the relative intensities of the overlapped bands of the two conformers. Nevertheless, because all predicted conformational isomerization barriers required to open the possibility of conversion of all the higher energy forms into the most stable *sa* conformer are small (below ~12 kJ $mol^{-1}$), a simulated spectrum was built in such a way that it represents the conversion of all the three higher energy conformers into the most stable *sa* form, starting from a matrix conformational composition equal to that of the deposited room temperature gas phase equilibrium. This simulated spectrum is shown in Fig. 4 (middle). It can be seen that it fits rather well the experimental difference spectrum, even though the spectra have relatively crowded regions exhibiting extensive band overlapping, which might lead to appearance of some 'artifacts' due to the subtraction procedures (these latter can be expected to be

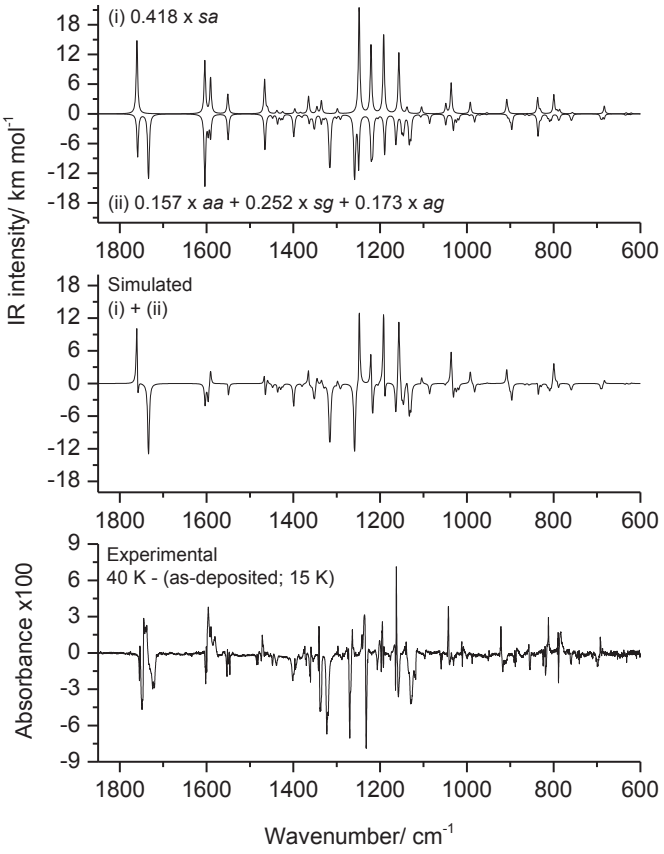


**Fig. 4.** *From bottom to top*: experimental difference infrared spectrum of CIQC (spectrum obtained after heating the matrix up to 40 K *minus* spectrum of the as-deposited matrix; 15 K), simulated difference spectrum showing the effect of conversion of *aa*, *sg* and *ag* conformers into the most stable *sa* form, and B3LYP/LANL2DZ+cc-pVDZ predicted spectra for *sa* (bands pointing up) and *aa*+*sg*+*ag* (bands pointing down), in both cases with intensities multiplied by the estimated gas phase equilibrium populations at room temperature.

influenced, for example, by the choice of the adopted fixed bandwidth in the simulated spectra, vs. the variable bandwidths of the experimental spectra).

Testifying the conversion of the remaining conformers into the *sa* conformer upon matrix warming, the described temperature variation results are a conclusive demonstration that the *sa* conformer is indeed the most stable conformer of the compound, both in the gas phase (as predicted by the calculations) and in the matrix media. Also, as pointed out above, these results robustly validate the used theoretical model in what concerns the prediction of energetic and vibrational data. Moreover, they also strongly facilitated the assignment of the spectral bands to the different conformers, which is provided in Table 2.

Some characteristic bands due exclusively to *syn*-type conformers (*sa* and *sg*) and *anti*-type (*aa* and *ag*) forms could be identified in the experimental spectra. The most intense of these characteristic bands are marked in Fig. 2. Besides the νC=O stretching region, where the *syn* conformers absorb within the 1755–1738 $cm^{-1}$ range and the *anti* forms between 1733 and ca. 1720 $cm^{-1}$, the bands at 1471, 1397 and 1341 $cm^{-1}$, in the 1202–1192 $cm^{-1}$ range, and at 1042/1040 and 699 $cm^{-1}$ are band marks ascribed to *syn* forms only, while those observed at 1484, 1401, 1337 and 1322 $cm^{-1}$, in the 1232–1206 $cm^{-1}$ region, and at 1032/1025 and 692 $cm^{-1}$, belong to *anti* conformers only (see also Table 2 for approximate description of the modes giving rise to these bands).

### 3.4. Single crystal X-ray diffraction results

The single-crystal XRD study performed at room temperature shows that in the crystal the CIQC molecule has a geometry close to that of the conformer predicted theoretically as the most stable for the isolated molecule (see also Section 3.4), a result that was also confirmed by the matrix-isolation investigation. In the crystal, the molecule has perfect $C_s$ symmetry as the molecules lie on the crystallographic mirror planes located at $z$=1/4 (and $z$=3/4) in the unit cell. The crystal structure consists at layers of molecules located on these mirror planes, the layer at $z$=3/4 being rotated around the origin by 60° with respect to the layer at $z$=1/4, as imposed by the crystallographic $6_3$ screw-axis running parallel to the *c*-axis (Fig. 5).

In each layer the main packing motif consists of a group of three molecules related by a three-fold rotation joined together by a weak C–H ⋯ O hydrogen-bond, the carbonyl O atom being an acceptor of an aromatic H atom of a neighbor molecule (Fig. 6). Interaction between this group of three molecules and neighbor groups in the same plane occurs mainly via a short contact between the iodine atom and an aromatic H atom of a neighbor molecule that could also be classified as a weak hydrogen bond. The arrangement of the molecules is such that the chlorine atoms are facing the center of the 3-molecule main motif and do not participate in any intermolecular hydrogen bond. An inspection of possible agents playing a role in intermolecular interactions between layers shows that the carbonyl oxygen atom is placed in a position as to act as possible acceptor of the 5-electron clouds of the aromatic rings of the molecules of the layers located above and below its own layer, although these interactions are probably weaker than the above mentioned C–H ⋯ O hydrogen bonds. Other interactions, such as those due to direct interaction between the 5-electron clouds of adjacent layers, appear to be even weaker due to less favorable geometry, as a significant slippage of the rings occurs when moving from one layer to the next layer.

### 3.5. Temperature variation IR studies for the neat solid compound

An interesting experimental strategy to spectroscopically investigate neat solid samples at cryogenic temperatures, under some conformational control, is to start by preparing a matrix of the compound to be studied and, then, allow the host matrix-atoms to evaporate, while allowing the guest molecules to diffuse and form a thin film of the substance. This procedure permits to know the conformational composition existing in the matrix immediately before the evaporation of the host atoms, which can be probed spectroscopically. One of the main advantages of the technique is that, in some cases, if desired, the conformational composition in the matrix can be very precisely manipulated (for example, through in situ narrowband selective infrared-induced conformational excitation),[40,41] thus allowing to investigate the effects of changing the pre-existing conformational mixture on the nature of the obtained neat solid phases.[42]

In the present study, this technique was successfully used to observe the conformational selection taken place upon crystallization of CIQC. The same argon matrix of the compound used to probe the conformational isomerization of the compound described before was subjected to further warming. As already mentioned, at 40 K the matrix sample showed partial conversion of the higher energy conformers into the most stable *sa* form (see Fig. 4). Nevertheless, the observed conformational conversion occurred only in a small extension (less than ~10%), so that, at 40 K, the matrix still contained a considerable amount of the higher-energy conformers. This can be seen clearly in Fig. 7, where the evolution of the infrared spectrum of the CIQC sample along the

**Table 2**
Assignment of the infrared spectra for matrix isolated ClQC (15 K), as well as for the neat solid glassy state and crystalline compound[a]

| Approximate description[b] | Experimental Ar matrix (15 K) ν | Glass (43 K) | Crystal (17 K)[c] | Calculated | | | | | | | |
|---|---|---|---|---|---|---|---|---|---|---|---|
| | | | | *sa* ν | $I^{IR}$ | *aa* ν | $I^{IR}$ | *sg* ν | $I^{IR}$ | *ag* ν | $I^{IR}$ |
| ν$CH_2$ *s* Ph | 3098.4 | 3097.4 | 3105.0 | 3157.2 | 1.1 | 3156.5 | 1.2 | 3157.6 | 1.1 | 3157.7 | 0.7 |
| νCH Ph | 3098.4 | 3097.4 | 3105.0 | 3153.0 | 0.3 | 3155.0 | 0.3 | 3154.3 | 0.3 | 3155.6 | 0.8 |
| ν$CH_2$ *as* Ph | 3071.7 | 3068.8 | 3088.1 | 3140.0 | 1.2 | 3138.0 | 1.1 | 3141.1 | 1.2 | 3139.6 | 1.0 |
| νCH Py | 3071.7 | 3068.8 | 3088.1 | 3132.9 | 2.3 | 3119.6 | 0.5 | 3132.7 | 2.2 | 3118.3 | 0.5 |
| ν$CH_3$ *as″* | 3003.4 | 2984.3 | | | | | | 3074.2 | 21.5 | 3075.1 | 19.5 |
| | 2998.3 | 2984.3 | 2991.0 | 3057.9 | 31.3 | 3060.5 | 29.5 | | | | |
| ν$CH_3$ *as′* | 2991.8 | 2984.3 | 2980.3 | 3051.8 | 22.8 | 3052.8 | 23.1 | 3054.4 | 6.9 | 3055.0 | 5.8 |
| ν$CH_2$ *as* | 2991.8 | 2984.3 | | | | | | 3045.0 | 23.3 | 3046.0 | 23.4 |
| | 2967.4 | 2945.2 | 2938.8 | 3025.7 | 7.0 | 3028.4 | 6.9 | | | | |
| ν$CH_2$ *s* | 2950.8 | 2945.2 | | | | | | 3007.0 | 32.1 | 3007.5 | 27.4 |
| | 2940.0 | 2932.4 | 2928.0 | 2985.8 | 18.5 | 2987.6 | 18.0 | | | | |
| ν$CH_3$ *s* | 2920.5 | 2908.9 | 2913.1 | 2975.1 | 17.2 | | | | | | |
| | 2917.0 | 2908.9 | | | | 2976.6 | 15.3 | 2973.8 | 17.8 | 2974.1 | 17.8 |
| νCO | 1754.8/1749.0/1747.4 | 1743.8 | | | | | | 1759.0 | 216.4 | | |
| | 1753.4/1744.8/1740.7/1738.3 | 1732.7 | 1733.9/1727.8 | 1760.7 | 224.5 | | | | | | |
| | 1732.6/1723.9/1720.2 | 1715.2 | | | | 1734.7 | 280.2 | | | 1733.4 | 270.2 |
| νC═C Ph | 1602.1 | 1597.2 | | | | 1603.8 | 151.9 | 1604.2 | 160.0 | 1604.0 | 152.9 |
| | 1595.8/1590.0 | 1591.5 | 1597.8/1590.1 | 1604.2 | 160.4 | | | | | | |
| νC═N Py | 1599.6 | 1582.8 | | | | 1596.6 | 63.2 | 1590.9 | 111.0 | 1596.3 | 66.4 |
| | 1581.4 | 1582.8 | 1584.4/1577.4 | 1590.9 | 107.5 | | | | | | |
| νC═C Ph | 1551.8 | 1548.9 | 1552.0/1548.7 | 1551.2 | 59.7 | 1550.1 | 60.8 | 1551.1 | 59.4 | 1550.0 | 60.8 |
| νC═C Py | 1484.0 | 1479.8 | | | | 1464.9 | 59.3 | | | 1464.9 | 55.3 |
| | 1471.3 | 1471.0 | 1466.1 | 1466.3 | 104.4 | | | 1465.9 | 114.6 | | |
| δ$CH_2$ | 1460.5 | 1471.0 | 1456.2 | 1459.8 | 13.7 | 1459.3 | 2.4 | | | | |
| | 1455.7 | 1448.0 | | | | | | 1447.6 | 7.2 | 1448.2 | 15.4 |
| δ$CH_3$ *as′* | 1448.2 | 1438.5 | 1436.6 | 1438.3 | 6.9 | 1438.5 | 1.2 | 1429.5 | 13.1 | 1436.6 | 33.4 |
| νCC Ph | 1448.2 | 1438.5 | 1436.6 | 1437.3 | 3.3 | 1436.1 | 28.1 | 1437.1 | 8.6 | 1429.0 | 15.1 |
| δ$CH_3$ *as″* | 1438.9 | n.obs | 1430.7 | 1424.8 | 6.3 | 1424.5 | 6.5 | 1424.8 | 10.6 | 1424.4 | 11.4 |
| νC═C Ph | 1401.4 | 1395.0 | | | | 1399.8 | 88.3 | | | 1398.7 | 87.7 |
| | 1397.1 | 1389.7 | 1391.0 | 1396.7 | 15.2 | | | 1396.4 | 15.8 | | |
| δ$CH_3$ *s* | 1387.8 | 1389.7 | 1385.0 | 1383.7 | 3.6 | 1383.6 | 8.7 | | | | |
| | 1383.6 | 1389.7 | | | | | | 1380.3 | 10.0 | 1379.3 | 4.8 |
| δCH Ph | 1374.1 | 1372.2 | 1372.0/1370.0 | 1365.1 | 53.4 | | | 1363.6 | 43.6 | | |
| | 1371.4 | 1372.2 | | | | 1360.1 | 3.1 | | | 1358.7 | 12.6 |
| | 1361.5 | 1359.9 | | | | 1351.3 | 68.0 | 1350.4 | 13.6 | 1353.3 | 54.1 |
| w$CH_2$ | 1359.7 | 1359.9 | 1357.2/1353.8 | 1345.7 | 20.4 | | | | | | |
| δCH Py | 1340.9 | 1339.2 | 1337.9 | 1335.5 | 39.1 | | | 1335.7 | 45.2 | | |
| | 1337.0 | 1321.7 | | | | 1329.2 | 10.5 | | | 1329.6 | 14.0 |
| νCC Py | 1322.4 | 1321.7 | | | | 1314.9 | 280.2 | | | 1317.1 | 248.4 |
| | 1297.8 | 1299.6 | 1302.3/1291.1 | 1298.7 | 15.1 | | | 1300.5 | 14.7 | | |
| tw $CH_2$ | 1287.9 | 1299.6 | | | | | | 1292.2 | 15.3 | 1290.7 | 15.4 |
| νC–O | 1270.3 | 1282.8 | | | | 1259.6 | 305.7 | | | 1258.1 | 253.8 |
| tw $CH_2$ | n.obs. | n.obs. | n.obs. | 1252.6 | 1.1 | 1253.1 | 1.1 | | | | |
| δCH Ph | 1266.7 | 1271.3 | 1271.7/1262.6 | 1248.5 | 321.3 | | | 1249.5 | 267.3 | | |
| δ$CH_2$ Ph | 1235.8 | 1232.0 [d] | 1228.2/1217.1 | 1221.1 | 208.9 | | | 1220.8 | 172.6 | | |
| | 1232.1 | | | | | 1218.4 | 154.4 | | | 1216.8 | 149.6 |
| δ$CH_2$ Ph | 1206.5 | | | | | 1205.1 | 3.0 | | | 1204.9 | 14.4 |
| νC–O | 1201.6/1195.5 | 1199.1 | 1197.9 | 1191.8 | 240.6 | | | | | | |
| | 1196.0/1192.3 | 1199.1 | | | | | | 1189.6 | 202.3 | | |
| γ$CH_2$ | 1164.7 | 1174.2 | | | | | | 1164.0 | 127.5 | 1161.9 | 65.7 |
| δ$CH_2$ Ph | 1163.0 | 1162.7 [d] | 1165.8 | 1156.8 | 184.5 | | | | | | |
| | 1157.9 | | | | | 1150.1 | 118.8 | 1146.7 | 66.5 | 1144.8 | 49.1 |
| γ$CH_2$ | 1143.4 | 1160.1 | 1161.2 | 1139.6 | 4.0 | 1138.6 | 4.5 | | | | |
| νCC Ph | 1140.0 | 1135.1 [d] | 1142.2 | 1137.9 | 16.4 | | | | | | |
| | 1129.0 | | | | | 1132.5 | 95.7 | 1133.3 | 76.1 | | |
| | 1119.6 | | | | | | | | | 1129.1 | 149.2 |
| ν$C–CH_3$ | 1117.6 | 1116.5 | 1118.2 | 1104.5 | 20.9 | 1106.4 | 21.7 | | | | |
| | 1097.4 | 1095.9 | | | | | | 1086.0 | 35.7 | 1085.7 | 17.7 |
| νCC Ph | 1058.2 | 1059.7 | 1063.8 | 1048.6 | 29.4 | 1048.3 | 22.1 | 1049.2 | 27.1 | 1048.5 | 22.5 |
| νO–C | 1042.5 | 1033.7 [d] | 1034.3 | 1036.3 | 93.5 | | | | | | |
| | 1040.7 | | | | | | | 1031.2 | 80.4 | | |
| | 1031.6 | | | | | 1024.3 | 54.0 | | | | |
| | 1025.4 | | | | | | | | | 1018.7 | 37.0 |
| δring Py | 1011.7 | 1009.8 | 1012.8 | 992.2 | 35.2 | 994.0 | 11.3 | | | | |
| | 999.9 | 1009.8 | | | | | | 982.0 | 31.4 | 982.8 | 15.7 |
| γ$CH_2$ *as* Ph | 963.1 | 998.5 | 1005.8 | 969.9 | 0.6 | 971.2 | 3.9 | 969.7 | 0.6 | 969.4 | 3.5 |
| γCH Py | 951.0 | 998.5 | | | | 965.0 | 0.6 | | | 963.9 | 1.7 |
| | 949.1 | 944.6 | 940.4 | 953.9 | 3.5 | | | 954.4 | 3.5 | | |
| νC–C(═O) | 921.6 | 922.4 | 922.4 | 908.1 | 42.3 | | | | | | |
| γCH Ph | 917.9 | 915.8 | 917.0 | 904.9 | 5.9 | 905.7 | 6.2 | 905.5 | 5.8 | 905.8 | 6.1 |
| νC–C(═O) | 911.1 | 910.0 | | | | 900.9 | 40.5 | | | | |
| | 889.0 | 885.8 | | | | | | 896.7 | 49.4 | 895.9 | 40.8 |

(*continued on next page*)

**Table 2** (*continued*)

| Approximate description[b] | Experimental Ar matrix (15 K) ν | Glass (43 K) | Crystal (17 K)[c] | Calculated | | | | | | | |
|---|---|---|---|---|---|---|---|---|---|---|---|
| | | | | *sa* ν | $I^{IR}$ | *aa* ν | $I^{IR}$ | *sg* ν | $I^{IR}$ | *ag* ν | $I^{IR}$ |
| γCH$_3$′ | 872.0 | 885.8 | | | | 866.2 | 9.2 | | | | |
| | 857.8 | 854.6 | 856.0 | 861.1 | 0.5 | | | | | | |
| | 855.2 | 846.9 | | | | | | 853.3 | 1.7 | 856.9 | 9.4 |
| νC–Cl | 819.7 | 825.0 | 838.4/824.6 | 836.9 | 48.9 | | | 836.6 | 47.5 | | |
| | 817.1 | 819.5/816.2 | | | | 835.7 | 52.9 | | | 835.6 | 52.4 |
| γCH$_2$ *s* Ph | 811.9 | 812.8 | 812.8 | 831.0 | 10.4 | 829.1 | 10.7 | 830.8 | 10.4 | 828.9 | 10.6 |
| δOCC | 790.0 | 785.5 | 790.8 | 799.6 | 57.8 | 805.3 | 38.8 | 809.2 | 30.5 | 813.7 | 22.5 |
| γCH$_3$″ | 783.9 | 774.5 | 788.7 | 792.2 | 7.9 | 792.8 | 3.8 | | | | |
| τring Ph | 776.0 | 759.7 | 760.1 | 786.3 | 11.6 | 785.7 | 16.0 | 789.1 | 18.5 | 787.5 | 19.9 |
| τring Ph | 760.0 | 755.9 | | | | | | 759.1 | 17.3 | 760.9 | 18.4 |
| γC=O | | 755.9 | 741.5 | 756.9 | 3.9 | 757.6 | 4.5 | 756.8 | 9.1 | 758.3 | 4.3 |
| δring Py | 699.2 | 698.3 | | | | 691.4 | 30.4 | | | 688.5 | 27.5 |
| | 691.7 | 689.5 | 689.4 | 683.3 | 23.6 | | | 683.5 | 22.9 | | |
| δring Ph | 634.1 | 635.1 | 635.1 | 632.8 | 3.2 | 634.5 | 3.5 | 633.3 | 2.9 | 635.4 | 3.3 |
| νC–I | n. obs. | 631.5 | 631.5 | 621.2 | 2.7 | 627.6 | 2.1 | 622.6 | 3.4 | 627.1 | 1.6 |
| γCCl | 595.6 | 593.5 | 593.4/589.5 | 596.3 | 1.8 | 595.0 | 1.8 | 596.4 | 2.2 | 595.7 | 2.3 |
| δCC=O | 573.6 | n.obs. | 579.3 | 567.4 | 7.6 | | | 564.9 | 7.9 | | |
| | 567.0 | n.obs. | | | | 556.9 | 2.7 | | | 557.6 | 2.2 |
| δCCl | 532.0 | 534.6 | 534.6 | 527.0 | 5.0 | 525.5 | 4.2 | 525.4 | 4.6 | 526.2 | 3.7 |

[a] Wavenumbers (ν) in cm$^{-1}$; calculated intensities ($I^{IR}$) in km mol$^{-1}$; the calculated wavenumbers were scaled by 0.978.
[b] ν, stretching; δ, bending; γ, rocking; w, wagging; tw, twisting; τ, torsion; Py, pyridine ring; Ph, Phenyl ring; *s*, symmetric; *as*, anti-symmetric.
[c] Assignments refer to the *sa* conformer, which constitutes the molecular unit in the crystal.
[d] Bands observed for the glassy phase at 1232.0, 1162.7, 1135.1 and 1033.7 cm$^{-1}$ exhibit very broad profiles and shall correspond to superposition of several bands belonging to different conformers present in this phase (in the Table the frequencies of these bands are presented in the first row of the set of rows to which they correspond, to avoid extensive repetition).

performed thermal treatment is shown. A selected spectral region is depicted in this figure, where the characteristic feature at ca. 1320 cm$^{-1}$ of conformers exhibiting the *anti* orientation of the ethyl carboxylic ester substituent in relation to the ring system (see Table 2) is highlighted in grey color. At 43 K, the argon evaporated and an amorphous thin film of CIQC was formed. The spectrum then obtained (see Fig. 7) shows the characteristic broad bands of a glassy state, and reveals the presence of the higher-energy conformers of the compound, testified by the presence of the 1320 cm$^{-1}$ band. This means that the fast evaporation of the argon atoms, together with the low temperature (i.e., very limited thermal energy accessible), precluded occurrence of an extensive conformational conversion. When reaching the temperature of 233 K, spectral changes started to be observed, which were completed when the temperature attained a temperature of 243 K. These changes indicated the progressive crystallization of the sample within the 233–243 K temperature range, and manifest in a generalized band narrowing and disappearance of the bands, which originate only in conformers other than the *sa* form (in Fig. 7, exemplified by the band at 1320 cm$^{-1}$). These observations demonstrated the conformational selection of the *sa* conformer upon crystallization, as also indicated by the X-ray diffraction data. The sample was then heated until 270 K and *re*-cooled back to 17 K, to allow for a crystal relaxation. The resulting infrared spectrum is shown in Fig. 8,

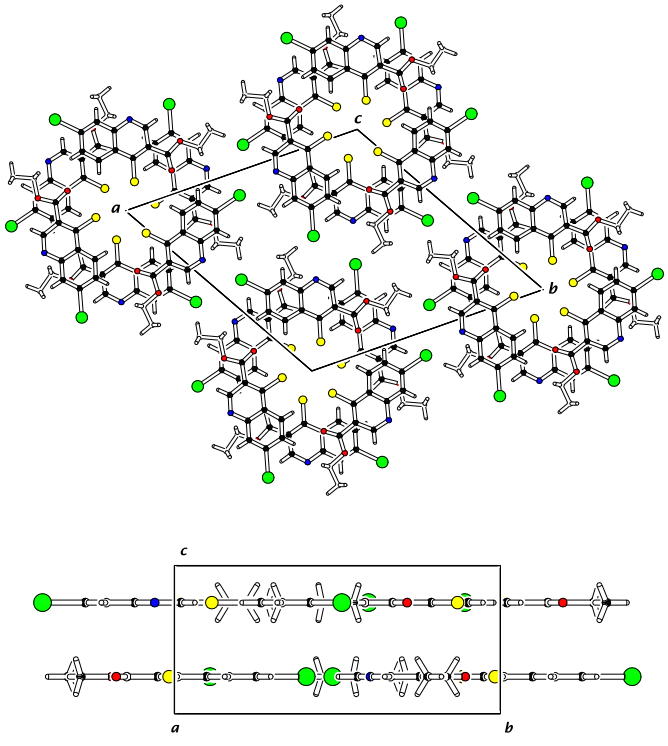


**Fig. 5.** *Top*: projection of the crystal structure along the *c*-axis showing the molecular packing diagram; *bottom*: projection along the *a*-axis, highlighting the layered nature of the molecular packing. (See Fig. S11 with an ORTEP plot of the molecule).

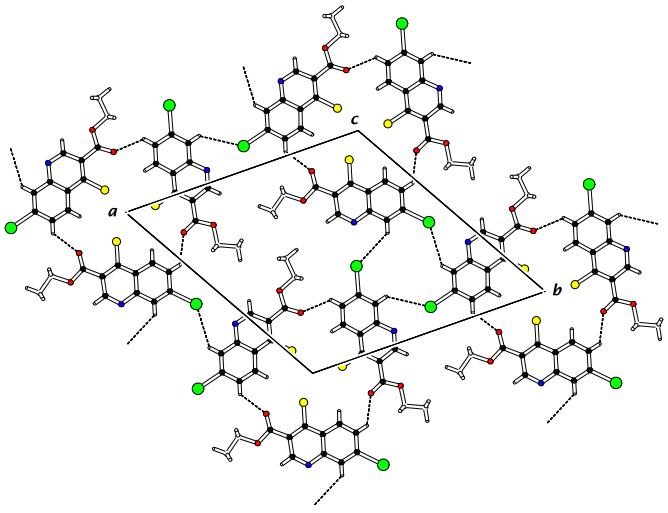


**Fig. 6.** Intermolecular hydrogen-bond interactions in the $z$=1/4 layer, depicted as dashed lines (C6–H6 ⋯ O1$^{(i)}$: 3.052(5) Å, $i$=−$x$+$y$,−$x$,−$z$+1/2; C8–H8 ⋯ I1$^{(ii)}$: 3.994(4) Å, ii=−$x$+$y$+1,−$x$+1, −$z$+1/2).

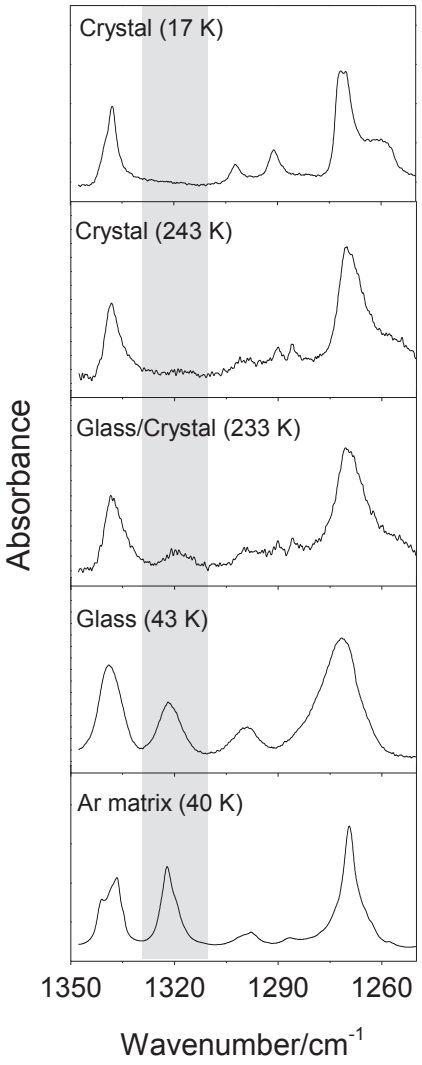


**Fig. 7.** Infrared spectra of ClQC obtained along the warming/cooling cycle. *From bottom to top*: spectrum of the argon matrix of the compound at 40 K; spectrum obtained at 43 K, after evaporation of the argon, corresponding to the spectrum of neat ClQC in a glassy state containing all conformers; spectrum obtained at 233 K, when the crystallization was taking place; spectrum of the crystal at 243 K; spectrum of the *re*-cooled crystal at 17 K. The shadow calls the attention to the disappearance of the band at *ca.* 1320 $cm^{-1}$ upon crystallization; this band is characteristic of the *aa* and *ag* conformers (see text).

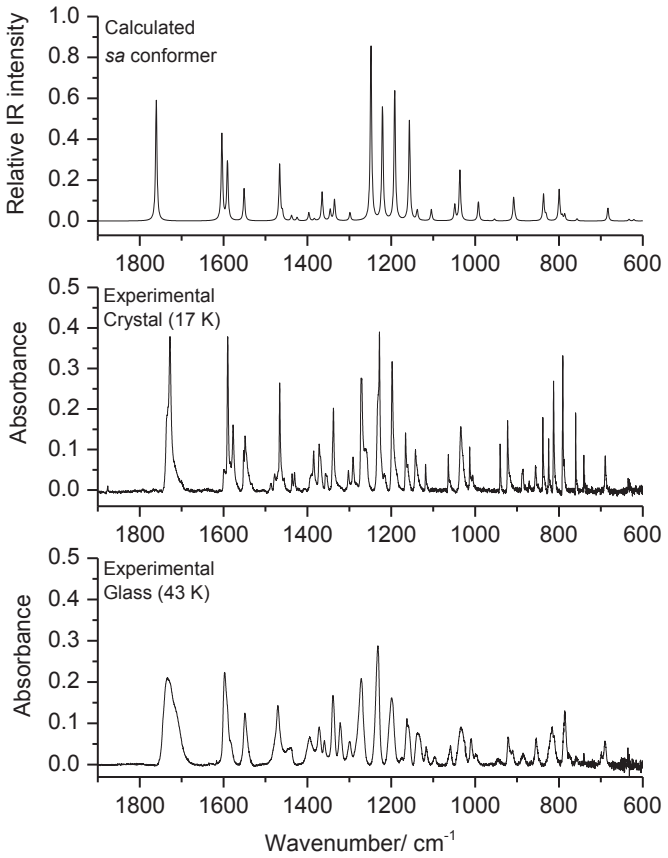


**Fig. 8.** *From bottom to top*: observed infrared spectrum of the ClQC amorphous solid, obtained at 43 K; spectrum of crystalline ClQC, at 17 K, and simulated infrared spectra using the B3LYP/LANL2DZ+cc-pVDZ calculated data for the most stable conformer (*sa*).

where it is compared with the spectrum of the glassy state (at 43 K) and also with the calculated spectrum of conformer *sa*. As expected taking into consideration the relatively weak intermolecular interactions present in the crystal of ClQC, the single molecule spectrum of the *sa* conformer reproduces generally well that of the crystalline sample (see also Table 2, with the assignments for the observed bands).

## 4. Conclusion

A new quinoline derivative, ethyl 4-chloro-7-iodoquinoline-3-carboxylate, a relevant intermediate for easy access to a range of new quinolone 3-esters, was synthesized and characterized structurally and vibrationally in both neat solid phases (low temperature amorphous and crystalline) and isolated in a cryogenic (~15 K) argon matrix. The performed theoretical calculations predicted existence of four different conformers of the molecule, all of them with significant populations in the gas phase at room temperature equilibrium. These four conformers were found to be present in the as-deposited Ar-matrix of the compound in relative amounts close to those predicted to exist in the rt gaseous beam used to prepare the matrix, and their vibrational signatures were obtained.

Upon annealing of the initially deposited matrix at higher temperatures (~40 K), conversion of the higher energy forms into the most stable conformer was found to take place, in consonance with the low predicted barriers for conformational isomerization.

Sublimation of the host matrix argon atoms (at ~43 K) resulted in the formation of an amorphous phase containing all four conformers. At T ~233–243 K, the amorphous rearranged to the crystalline state, whose molecular unit corresponds to the most stable ClQC conformer. The crystal belongs to the hexagonal $P6_3/m$ space group, with $a=b=17.7928(2)$ Å, and $c=6.9830(1)$ Å, at room temperature. The molecules lie on a crystallographic mirror plane and are stacked in layers along the *c*-axis, the main packing motif consisting of a group of three molecules related by a three-fold rotation and joined together by three weak C–H ··· O hydrogen-bonds.

A range of quinolone 3-esters **1** (Scheme 1) have been prepared and tested in vitro against *P. falciparum* malaria parasites.[20] Interestingly, some seven-substituted derivatives expressed activity at low nanomolar concentrations, emerging as leads for malaria chemotherapy.[20] It was proposed that quinolone 3-esters target the $Q_o$ site of the enzyme in the *bc1* complex, leading to a drop of mitochondrial function,[18,19] collapse of the *trans*-membrane electrochemical potential and parasite death.[20] Structure–activity relationship studies on the quinolone 3-ester chemotype and docking studies performed *in silico* at the yeast $Q_o$ site of the *bc1* protein complex of *P. falciparum* indicated that both the 4-oxoquinoline and

the ethyl ester moieties are relevant for activity.[20] The present work shows that the barriers predicted for conformational isomerization around the ethyl ester moiety in CIQC are low. These low barriers may be important to facilitate structural adjustments of the ethyl ester moiety in the enzyme pocket, to maximize drug-target interactions and, thus, improve the pharmacokinetic profile.

## Acknowledgements

The authors gratefully acknowledge *Fundação para a Ciência e a Tecnologia* (FCT), through the projects PEst-OE/QUI/UI0313/2014 (Coimbra Chemistry Centre) and PEst-CCMAR/Multi/04326/2013 (Center of Marine Sciences, CCMAR), cofunded by QREN-COMPETE-UE. Financial support has also been provided within the framework of the FCT post-doctoral grant SFRH/BPD/88372/2012 (N. K.) and the doctoral grant SFRH/BD/81821/2011 (P. H.). NMR spectrometers used are part of The National NMR Facility, supported by FCT (RECI/BBB-BQB/0230/2012).

## Supplementary data

Supplementary data (Figs. S1–S8, with $^{1}$H NMR, $^{13}$C NMR and MS spectra of **4**, OQIC and CIQC; Figs. S9 and S10, with the B3LYP/LANL2DZ+cc-pVDZ calculated potential energy profiles for conformational isomerization in CIQC; Fig. S11, with an ORTEP plot of the molecule showing the atomic numbering scheme; Table S1, with the calculated wavenumbers and infrared intensities for the four investigated conformers of the compound; Crystallographic Data Section (Tables CDS1–CDS9), with the results of the crystallographic single-crystal XRD study.) associated with this article can be found in the online version, at http://dx.doi.org/10.1016/j.tet.2015.07.076.

## References and notes

1. Nakamura, S.; Kozuka, M.; Bastow, K. F.; Tokuda, H.; Nishino, H.; Suzuki, M.; Tatsuzaki, J.; Morris Natschke, S. L.; Kuo, S.-C.; Lee, K.-H. *Bioorg. Med. Chem.* **2005**, *13*, 4396–4401.
2. Tedesco, R.; Shaw, A. N.; Bambal, R.; Chai, D.; Concha, N. O.; Darcy, M. G.; Dhanak, D.; Fitch, D. M.; Gates, A.; Gerhardt, W. G.; Halegoua, D. L.; Han, C.; Hofmann, G. A.; Johnston, V. K.; Kaura, A. C.; Liu, N.; Keenan, R. M.; Lin-Goerke, J.; Sarisky, R. T.; Wiggall, K. J.; Zimmerman, M. N.; Duffy, K. J. *J. Med. Chem.* **2006**, *49*, 971–983.
3. Kumar, D. V.; Rai, R.; Brameld, K. A.; Somoza, J. R.; Rajagopalan, R.; Janc, J. W.; Xia, Y. M.; Ton, T. L.; Shaghafi, M. B.; Hu, H.; Lehoux, I.; To, N.; Young, W. B.; Green, M. J. *Bioorg. Med. Chem. Lett.* **2011**, *21*, 82–87.
4. Serrão, E.; Debnath, B.; Otake, H.; Kuang, Y.; Christ, F.; Debyser, Z.; Neamati, N. *J. Med. Chem.* **2013**, *56*, 2311–2322.
5. Dorow, R. L.; Herrinton, P. M.; Hohler, R. A.; Maloney, M. T.; Mauragis, M. A.; McGhee, W. E.; Moeslein, J. A.; Strohbach, J. W.; Veley, M. F. *Org. Process Res. Dev.* **2006**, *10*, 493–499.
6. Sultana, N.; Naz, A.; Khan, B.; Arayne, M. S.; Mesaik, M. A. *Med. Chem. Res.* **2009**, *19*, 1210–1221.
7. Kathrotiya, H. G.; Patel, M. P. *Eur. J. Med. Chem.* **2013**, *63*, 675–684.
8. Pidathala, C.; Amewu, R.; Pacorel, B.; Nixon, G. L.; Gibbons, P.; Hong, W. D.; Leung, S. C.; Berry, N. G.; Sharma, R.; Stocks, P. A.; Srivastava, A.; Shone, A. E.; Charoensutthivarakul, S.; Taylor, L.; Berger, O.; Mbekeani, A.; Hill, A.; Fisher, N. E.; Warman, A. J.; Biagini, G. A.; Ward, S. A.; O'Neill, P. M. *J. Med. Chem.* **2012**, *55*, 1831–1843.
9. Leung, S. C.; Gibbons, P.; Amewu, R.; Nixon, G. L.; Pidathala, C.; Hong, W. D.; Pacorel, B.; Berry, N. G.; Sharma, R.; Stocks, P. A.; Srivastava, A.; Shone, A. E.; Charoensutthivarakul, S.; Taylor, L.; Berger, O.; Mbekeani, A.; Hill, A.; Fisher, N. E.; Warman, A. J.; Biagini, G. A.; Ward, S. A.; O'Neill, P. M. *J. Med. Chem.* **2012**, *55*, 1844–1857.
10. Biagini, G. A.; Fisher, N.; Shone, A. E.; Mubaraki, M. A.; Srivastava, A.; Hill, A.; Antoine, T.; Warman, A. J.; Davies, J.; Pidathala, C.; Amewu, R. K.; Leung, S. C.; Sharma, R.; Gibbons, P.; Hong, D. W.; Pacorel, B.; Lawrenson, A. S.; Charoensutthivarakul, S.; Taylor, L.; Berger, O.; Mbekeani, A.; Stocks, P. A.; Nixon, G. L.; Chadwick, J.; Hemingway, J.; Delves, M. J.; Sinden, R. E.; Zeeman, A. M.; Kocken, C. H.; Berry, N. G.; O'Neill, P. M.; Ward, S. A. *Proc. Natl. Acad. Sci. U.S.A.* **2012**, *109*, 8298–8303.
11. Cowley, R.; Leung, S.; Fisher, N.; Al-Helal, M.; Berry, N. G.; Lawrenson, A. S.; Sharma, R.; Shone, A. E.; Ward, S. A.; Biagini, G. A.; O'Neill, P. M. *Medchemcomm* **2012**, *3*, 39–44.
12. World Malaria Report 2014; World Health Organization, 2014.
13. Shetty, N.; Tang, J. W.; Andrews, J. *Infectious Disease: Pathogenesis, Prevention and Case Studies*; John Wiley & Sons, 2009.
14. Noedl, H.; Se, Y.; Schaecher, K.; Smith, B. L.; Socheat, D.; Fukuda, M. M. *N. Engl. J. Med.* **2008**, *359*, 2619–2620.
15. Menard, D.; Ariey, F. *Lancet Infect. Dis.* **2015**, *15*, 367–368.
16. Barton, V.; Fisher, N.; Biagini, G. A.; Ward, S. A.; O'Neill, P. M. *Curr. Opin. Chem. Biol.* **2010**, *14*, 440–446.
17. Mitchell, P. *FEBS Lett.* **1975**, *59*, 137–139.
18. Hammond, D. J.; Burchell, J. R.; Pudney, M. *Mol. Biochem. Parasitol.* **1985**, *14*, 97–109.
19. Painter, H. J.; Morrisey, J. M.; Mather, M. W.; Vaidya, A. B. *Nature* **2007**, *446*, 88–91.
20. Biagini, G. A.; Viriyavejakul, P.; O'Neill, P. M.; Bray, P. G.; Ward, S. A. *Antimicrob. Agents Chemother.* **2006**, *50*, 1841–1851.
21. Frisch, M. J.; Trucks, G. W.; Schlegel, H. B.; Scuseria, G. E.; Robb, M. A.; Cheeseman, J. R.; Scalmani, G.; Barone, V.; Mennucci, B.; Petersson, G. A.; Nakatsuji, H.; Caricato, M.; Li, X.; Hratchian, H. P.; Izmaylov, A. F.; Bloino, J.; Zheng, G.; Sonnenberg, J. L.; Hada, M.; Ehara, M.; Toyota, K.; Fukuda, R.; Hasegawa, J.; Ishida, M.; Nakajima, T.; Honda, Y.; Kitao, O.; Nakai, H.; Vreven, T.; Montgomery, J. A., Jr.; Peralta, J. E.; Ogliaro, F.; Bearpark, M.; Heyd, J. J.; Brothers, E.; Kudin, K. N.; Staroverov, V. N.; Kobayashi, R.; Normand, J.; Raghavachari, K.; Rendell, A.; Burant, J. C.; Iyengar, S. S.; Tomasi, J.; Cossi, M.; Rega, N.; Millam, J. M.; Klene, M.; Knox, J. E.; Cross, J. B.; Bakken, V.; Adamo, C.; Jaramillo, J.; Gomperts, R.; Stratmann, R. E.; Yazyev, O.; Austin, A. J.; Cammi, R.; Pomelli, C.; Ochterski, J. W.; Martin, R. L.; Morokuma, K.; Zakrzewski, V. G.; Voth, G. A.; Salvador, P.; Dannenberg, J. J.; Dapprich, S.; Daniels, A. D.; Farkas, Ö.; Foresman, J. B.; Ortiz, J. V.; Cioslowski, J.; Fox, D. J. *Gaussian 09, Revision A.02*; Gaussian: Wallingford, CT, 2009.
22. Becke, A. D. *Phys. Rev. A* **1988**, *38*, 3098–3100.
23. Lee, C.; Yang, W.; Parr, R. G. *Phys. Rev. B* **1988**, *37*, 785–789.
24. Vosko, S. H.; Wilk, L.; Nusair, M. *Can. J. Phys.* **1980**, *58*, 1200–1211.
25. Dunning, T. H. *J. Chem. Phys.* **1989**, *90*, 1007–1023.
26. Davidson, E. R. *Chem. Phys. Lett.* **1996**, *260*, 514–518.
27. Hay, P. J.; Wadt, W. R. *J. Chem. Phys.* **1985**, *82*, 299–310.
28. Gould, R. G.; Jacobs, W. A. *J. Am. Chem. Soc.* **1939**, *61*, 2890–2895.
29. Riveros, J. M. *J. Chem. Phys.* **1967**, *46*, 4605–4612.
30. Lister, D. G.; Owen, N. L.; Palmieri, P. *J. Mol. Struct.* **1976**, *31*, 411–413.
31. Fausto, R.; Teixeira-dias, J. J. C. *J. Mol. Struct. THEOCHEM* **1987**, *150*, 381–389.
32. Fausto, R. *J. Mol. Struct. THEOCHEM* **1994**, *315*, 123–136.
33. Redondo, M. I.; Garcia, M. V.; Raso, M. A.; Luck, W. A. P. *J. Mol. Struct.* **1990**, *218*, 213–218.
34. Fausto, R.; De Carvalho, L. A. E. B.; Teixeira-Dias, J. J. C. *J. Comput. Chem.* **1992**, *13*, 799–809.
35. Teixeira-Dias, J. J. C.; Fausto, R. *A Molecular Mechanics Force Field for Conformational Analysis of Simple Acylchlorides, Carboxylic and Esters*, 1986.
36. Barnes, A. J. *J. Mol. Struct.* **1984**, *113*, 161–174.
37. Reva, I. D.; Stepanian, S. G.; Adamowicz, L.; Fausto, R. *Chem. Phys. Lett.* **2003**, *374*, 631–638.
38. Reva, I.; Simão, A.; Fausto, R. *Chem. Phys. Lett.* **2005**, *406*, 126–136.
39. Reva, I. D.; Lopes de Jesus, A. J.; Rosado, M. T. S.; Fausto, R.; Eusébio, M. E.; Redinha, J. S. *Phys. Chem. Chem. Phys.* **2006**, *8*, 5339–5349.
40. Sharma, A.; Reva, I.; Fausto, R. *J. Am. Chem. Soc.* **2009**, *131*, 8752–8753.
41. Lapinski, L.; Nowak, M. J.; Reva, I.; Rostkowska, H.; Fausto, R. *Phys. Chem. Chem. Phys.* **2010**, *12*, 9615–9618.
42. Hakala, M.; Marushkevich, K.; Khriachtchev, L.; Hämäläinen, K.; Räsänen, M. *J. Chem. Phys.* **2011**, *134*, 054506(1)–054506(7).